

# Molecular dynamics under the confinement by the host lattice in zeolitic adsorbate–adsorbent systems

Reinhold Haberlandt\*, Jörg Kärger

Universität Leipzig, Fakultät für Physik und Geowissenschaften, Linnéstr. 5, D-04103, Leipzig, Germany

## Abstract

Molecular diffusion in the pore system of zeolites exhibits a number of peculiarities which do not occur in bulk liquids. Examples are presented, discussed by using both analytical methods and MD simulations and compared with results of experimental studies. The influence of different input parameters is discussed. © 1999 Elsevier Science S.A. All rights reserved.

*Keywords:* Molecular dynamics; Adsorbate; Adsorbent

## 1. Introduction

As a unique feature of zeolitic adsorbate–adsorbent systems, intracrystalline molecular propagation proceeds under well-defined steric confinement.

As an example, Fig. 1 shows the structure of a zeolite of type LTA. It consists of large cavities in simple cubic arrangement. The upper part provides an impression of the position of the atoms in the zeolite structure, while the lower part gives a simplified representation in which the silicon and aluminium atoms are indicated by the points of intersection between the solid lines. For a better visualization of the structure, the planes formed by the aluminium–silicon-4-rings and 6-rings are shaded. An alternative way of structure visualization is shown in Fig. 2. This presentation shows a zeolite of type MFI (with the representatives ZSM-5 and silicalite), which consists of a network of sinusoidal and straight channels in  $x$  and  $y$  direction, respectively.

As a consequence of the confinement by the internal surface, zeolitic diffusion reveals a number of peculiarities which have no correspondence in the bulk fluid. These peculiarities include the existence of structure-related propagators, the mutual dependence of the rate of propagation in different crystallographic directions, the deviation from normal diffusion in perfectly ordered systems and the dominating role of the guest–host interaction in molecular propagation. Each of these peculiarities are considered in more detail in this contribution.

The presentation is mainly based on the application of molecular dynamics (MD) simulations and analytical methods. In the last section the influence of changing different input parameters (potential, model) is discussed. Wherever possible, the results are compared with the information provided by experimental methods.

## 2. Structure-related propagator

The internal dynamics of fluid systems is most informatively represented by the propagator  $P(\mathbf{r}, t | \mathbf{r}_0, 0)$ , which denotes the (conditional) probability density that a molecule, initially at position  $\mathbf{r}_0$ , will have got to position  $\mathbf{r}$  at time  $t$ . Experimentally accessible is the averaged propagator

$$P(\mathbf{r}, t) = \int p(\mathbf{r}_0) P(\mathbf{r}_0 + \mathbf{r}, t | \mathbf{r}_0, 0) d\mathbf{r}_0, \quad (1)$$

where  $p(\mathbf{r}_0)$  denotes the probability density of finding a molecule at position  $\mathbf{r}_0$ . The averaged propagator represents the probability distribution of molecular displacements  $\mathbf{r}$  during the time interval  $t$  for an arbitrarily selected molecule within the sample under study. The pulsed field gradient (PFG) NMR technique [1] allows the determination of the averaged propagator [2,3] over time and space scales of typically milliseconds and micrometers. In quasielastic neutron scattering (QENS) – with the relevant time and space scales of 1–100 ps and nanometers –, the averaged propagator  $P(\mathbf{r}, t)$  is generally referred to as the self-part  $G_s(\mathbf{r}, t)$  of the van Hove auto-correlation function  $G(\mathbf{r}, t)$  [4–14]

\*Corresponding author. Tel.: +49-341-2352280; fax: +49-341-2352307; e-mail: reinhold.haberlandt@physik.uni-leipzig.de

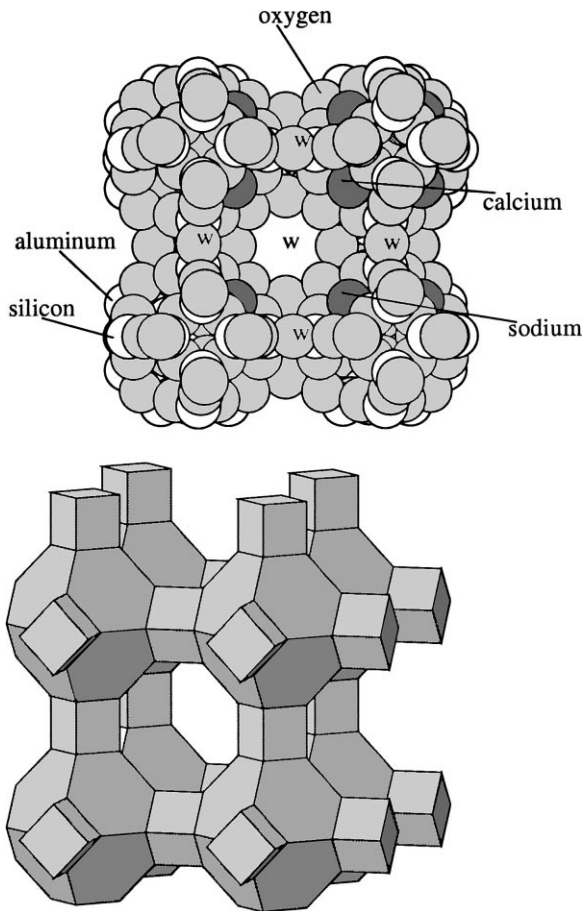


Fig. 1. Structure of zeolites of type LTA (left: internal view, atoms, windows (w); right: general view, cavities, windows).

$$G(\mathbf{r}, t) = \frac{1}{N} \left\langle \sum_{j=1}^N \sum_{\ell=1}^N \delta[\mathbf{r} + \mathbf{r}_\ell(0) - \mathbf{r}_j(t)] \right\rangle, \quad (2)$$

with  $N$  denoting the particle number. For distinguishable particles one can split  $G(\mathbf{r}, t)$  into the self-part  $G_s$  and the distinct-part  $G_d$

$$G_s(\mathbf{r}, t) = \frac{1}{N} \left\langle \sum_{j=1}^N \delta[\mathbf{r} + \mathbf{r}_j(0) - \mathbf{r}_j(t)] \right\rangle, \quad (3)$$

$$G_d(\mathbf{r}, t) = \frac{1}{N} \left\langle \sum_{j=1}^N \sum_{\ell=1(\neq j)}^N \delta[\mathbf{r} + \mathbf{r}_\ell(0) - \mathbf{r}_j(t)] \right\rangle, \quad (4)$$

where  $G_s$  correlates positions of the same particle ( $j=\ell$ ) at different times while  $G_d$  correlates positions of different ones ( $j \neq \ell$ ).  $G_s(\mathbf{r}, t)$  gives the probability density that within time  $t$  a particle moves by  $\mathbf{r}$ , while  $G_d(\mathbf{r}, t)$  gives the probability density of finding any different particle at distance  $\mathbf{r}$  from the former position of some particle.

In a homogeneous system, the propagator  $P(\mathbf{r}, t)$  (Eq. (1)) is easily found to be a Gaussian

$$P(\mathbf{r}, t) = (4\pi Dt)^{-3/2} \exp(-r^2/(4Dt)), \quad (5)$$

with  $D$  denoting the self-diffusivity.

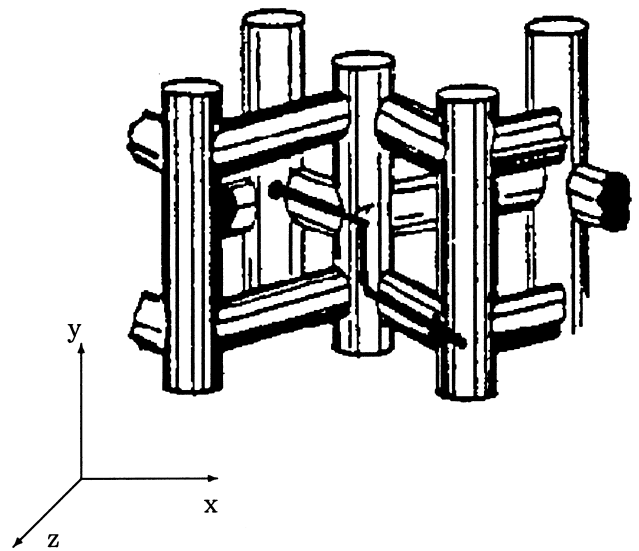


Fig. 2. Structure of zeolites of type MFI. The indicated diffusion path allows molecular propagation in the  $z$ -direction by subsequent steps in the  $x$  and  $y$  directions (cf. Section 3).

The evolution of the probability of particle displacements as contained in the spatial-temporal dependence of the propagator, corresponding to Eq. (5), is shown in Fig. 3 (top).

In such representations one is clearly confined to show the propagator with respect to one coordinate only. Fig. 3 (bottom) illustrates that the heterogeneity of the host system leads to a fine-structure of the propagator with spacings given by the separation between adjacent pore centres. The propagator in Fig. 3 (bottom) has been determined by MD simulations for methane in a cation-free A-type zeolite (for short: ZK4) for potential set B (see Table 1), loading  $I=3$  (throughout this paper given in molecules per supercage) and temperature  $T=300$  K [15].

Fig. 4 uses an alternative representation of the propagator for demonstrating the diffusion behaviour of ethane in ZK4 in a time interval of  $t=1-1000$  ps [16,17]. In this case, the propagator was calculated with respect to two coordinates  $x$ ,  $y$ . It is to be seen that the propagator shows a more complicated structure than in the case of  $\text{CH}_4$ , most likely

Table 1  
Parameter sets used for the LJ (12,6) potential (Eq. (20))

Zeolite		$\sigma$ (Å)	$\epsilon$ (kJ mol <sup>-1</sup> )
LTA	CH <sub>4</sub> -CH <sub>4</sub>	3.817	1.232
LTA	CH <sub>4</sub> -Si	2.14	0.29
LTA	CH <sub>4</sub> -O (set A)	3.14	1.5
LTA	CH <sub>4</sub> -O (set B)	3.46	0.81
LTA	C <sub>2</sub> H <sub>6</sub> -O	3.775	1.536
Silicalite	CH <sub>4</sub> -CH <sub>4</sub>	3.730	1.230
Silicalite	CH <sub>4</sub> -O	3.214	1.108
Silicalite	Xe-Xe	4.064	1.870
Silicalite	Xe-O	3.296	1.679

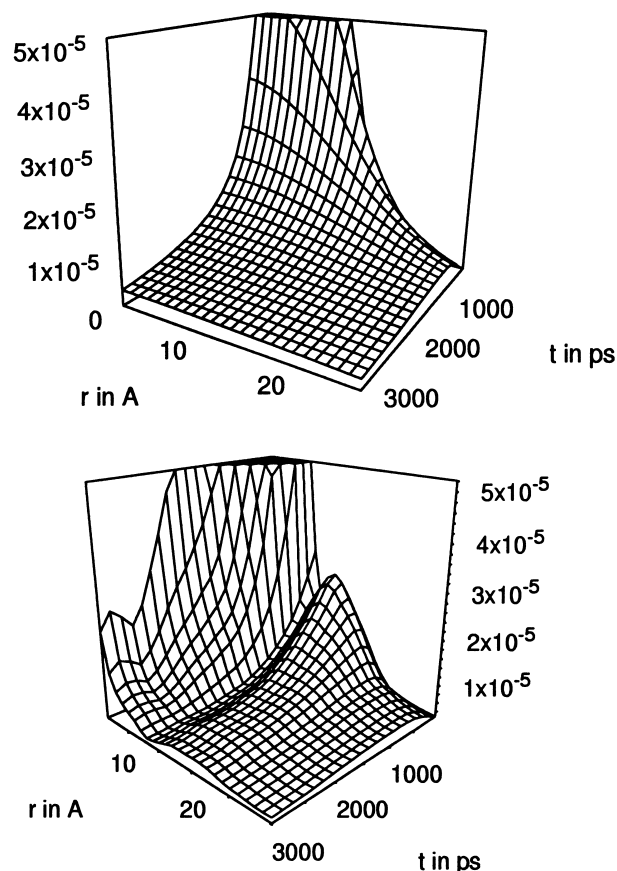


Fig. 3. Propagator  $P(\mathbf{r}, t)$  (Eq. (1)) in an ideal bulk system (top) and in ZK4 (bottom) with the same self-diffusivities ( $D=6 \times 10^{-9} \text{ m}^2 \text{ s}^{-1}$ ).

as a consequence of the more intricate intermolecular interaction.

The specific structurization of the propagators (see Fig. 3 (bottom) and Fig. 4) is caused by the reflections of the guest molecules at the walls of the cavities in the zeolites which yield peaks in the correlation functions. For an ideal zeolite lattice, the periodicity of the propagator is conserved over arbitrarily large space and time scales. This is demonstrated by Fig. 5.

For zeolites of non-cubic structure, the propagator exhibits the differences of molecular propagation in different directions. This is exemplified by Fig. 6 showing the propagator with respect to the  $x$ -,  $y$ - and  $z$ -axis (cf. Fig. 1, top) for methane in silicalite.

The structurization of the propagator is an immediate consequence of the periodicity of the particle distribution in space caused by the zeolite pore structure. It is not unexpected, therefore, that the propagator may be factorized in a contribution of the type of Eq. (5) and the spatial auto-correlation function of molecular distribution, yielding [11–14]

$$P(z, t) = (4\pi Dt)^{-1/2} \exp(-z^2/(4Dt)) \langle p(z_0) p(z_0 + z) \rangle_{z_0}, \quad (6)$$

where  $p(z_0)$  denotes the probability density of finding a molecule with the  $z$  coordinate  $z_0$ , and  $\langle \dots \rangle_{z_0}$  is the ensemble average about all possible initial states  $z_0$ . The quality of this approximation is visualized by Fig. 7, which compares the exact propagator as following directly from the simulation (right-hand side) with that determined on the basis of Eq. (6) (left-hand side [11,14]).

Figs. 5 and 6 demonstrate the decay of the Gaussian-like curves – modulated by the lattice periodicity – with respect to time. One should note the parabolic form due to  $\langle x^2 \rangle$ ,  $\langle y^2 \rangle$ ,  $\langle z^2 \rangle \sim t$ . Moreover, from the decay of the curvatures in Fig. 6 one can see that the diffusion coefficients in the different directions  $x$ ,  $y$  and  $z$  obey the relation  $D_y > D_x > D_z$ . This sequence indicates that the mobility is highest in the straight channels, moderate in the zig-zag channels and smallest in  $z$ -direction due to the necessity of detours of the guest molecules.

Since the relevant space scale is in the nanometer range, among the experimental techniques only QENS provides the potential of experimentally confirming the theoretical prediction of the structurized propagator. As a consequence of the limited sensitivity, however, in contrast to PFG NMR [2], QENS has so far not been applied to determining propagators directly from the primary experimental data. In general, the information about transport characteristics have been deduced by fitting the solutions for certain models to the experimental data. Knowing the propagator as resulting from the MD simulations, one may clearly determine theoretically the primary experimental data, which would correspond to it. As an example, Fig. 8 shows the dynamic structure factor  $S(\mathbf{k}, \omega)$  ( $\mathbf{k}$  – wave vector,  $\omega$  – frequency) which is related to the propagator (self-part of the van Hove function) by the relation:

$$S(\mathbf{k}, \omega) = \frac{1}{2\pi} \int_{-\infty}^{\infty} \int P(\mathbf{r}, t) e^{-i(\mathbf{k}\mathbf{r} - \omega t)} d\mathbf{r} dt. \quad (7)$$

Fig. 9 shows the intermediate scattering function  $F(\mathbf{k}, t)$  [11,14]) of QENS, which is defined by

$$F(\mathbf{k}, t) = \int P(\mathbf{r}, t) e^{-i\mathbf{k}\mathbf{r}} d\mathbf{r}, \quad G_s(\mathbf{r}, t) \equiv P(\mathbf{r}, t) \quad (8)$$

using the propagator of methane in cation-free zeolite LTA as represented in Figs. 4 and 7 and [11,14]. The scattering vector  $\mathbf{k}$  has been chosen to be parallel to one of the crystallographic axes.

As a remarkable feature of the intermediate scattering function, a pronounced peak is observed at  $\mathbf{k}a=2\pi$ , where  $a$  ( $=1.23 \text{ nm}$ ) is the lattice constant of zeolite A.

In QENS experiments one has clearly to do with powder samples. This leads to the formation of much less pronounced maxima than exhibited in Fig. 4, and, consequently, in Fig. 9. The experimental observation of such maxima is a challenging task for QENS. In the light of the present study, such a behaviour is to be quite generally expected as a consequence of the structured propagator,

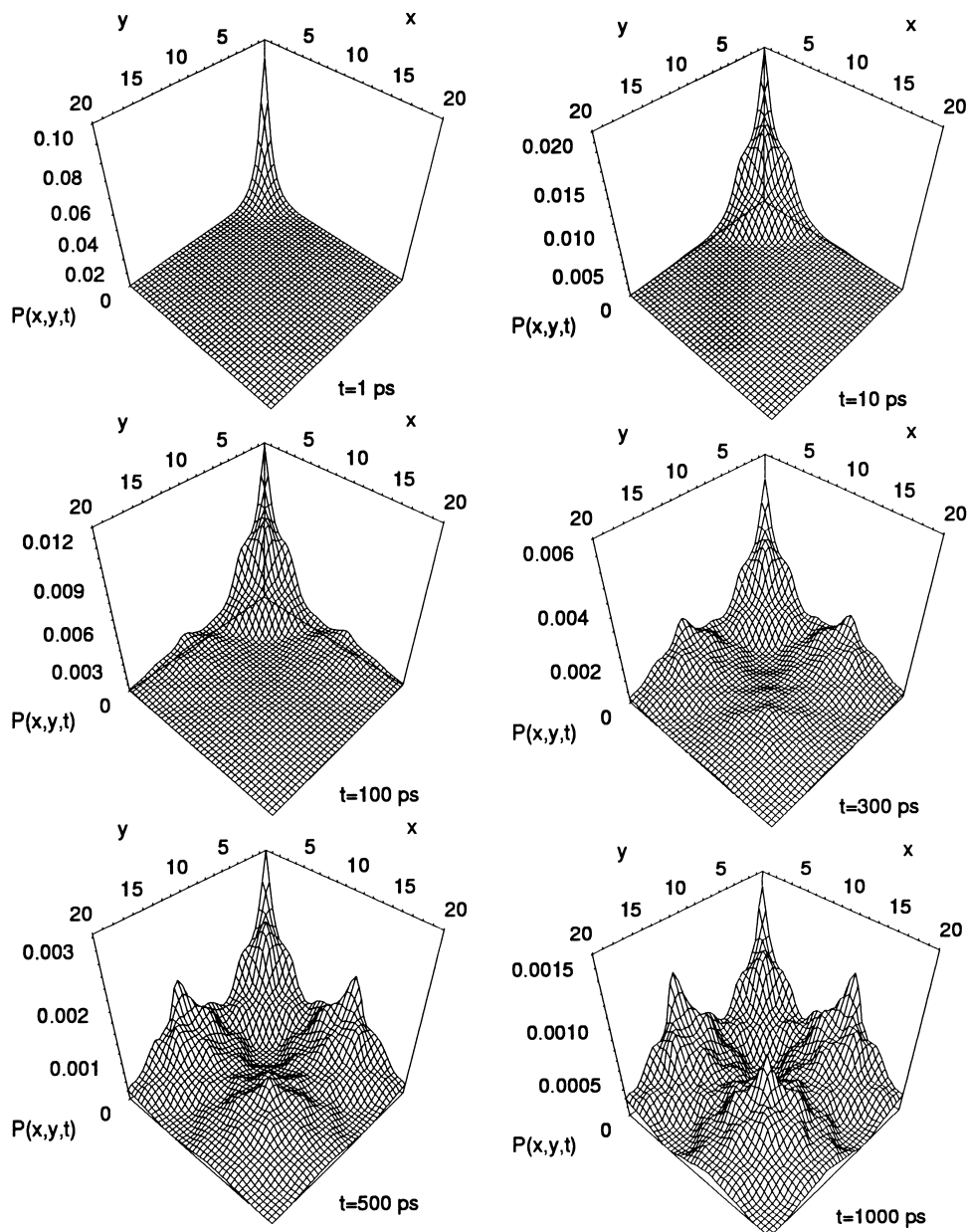


Fig. 4. Two-dimensional graph of the time development of the propagator  $P(x, y, t) - x, y$  in Å;  $t$  in ps – calculated from a trajectory (potential set A (see Table 1,  $I=3$ ,  $T=300$  K,  $D=2 \times 10^{-9} \text{m}^2 \text{s}^{-1}$ ) [16].

which is caused by the heterogeneity of the distribution of the diffusants in space.

### 3. Correlation rules of zeolitic diffusion

The existence of a well-defined network of channels and/or pores implies that molecular displacements into different directions are not independent of each other. A typical example of this correlated motion has been provided by Fig. 2. The indicated diffusion path demonstrates that in silicalite molecular displacement in  $z$ -direction only occurs by subsequent displacements along

the channels in  $x$ - and  $y$ -direction. Under the supposition that subsequent displacements from one channel intersection to an adjacent one are independent of each other, i.e. that the particle ‘memory’ is much shorter than the diffusion time from one intersection to the next one, the diffusivities in  $x$ -,  $y$ - and  $z$ -direction have been shown to be related to each other by reciprocal addition [18,19], yielding

$$\frac{c^2}{D_z} = \frac{a^2}{D_x} + \frac{b^2}{D_y} \quad (9)$$

with  $a$ ,  $b$ ,  $c$  and  $D_x$ ,  $D_y$ ,  $D_z$  denoting the extensions of the unit cell and the diffusivities in  $x$ -,  $y$ - and  $z$ -direction, respec-

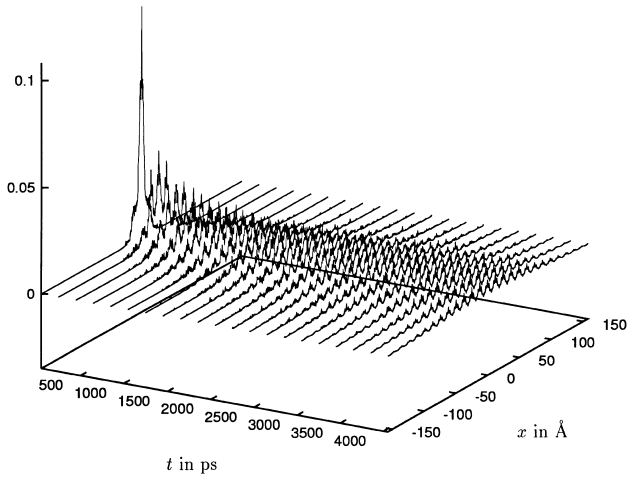


Fig. 5. The propagator  $P(x, t)$  (or self-part  $G_s(x, t)$  (Eq. (3)) of the van Hove correlation function) for diffusion of methane in ZK4 at  $I=3$  and  $T=300$  K,  $D=6 \times 10^{-9} \text{ m}^2 \text{ s}^{-1}$ .

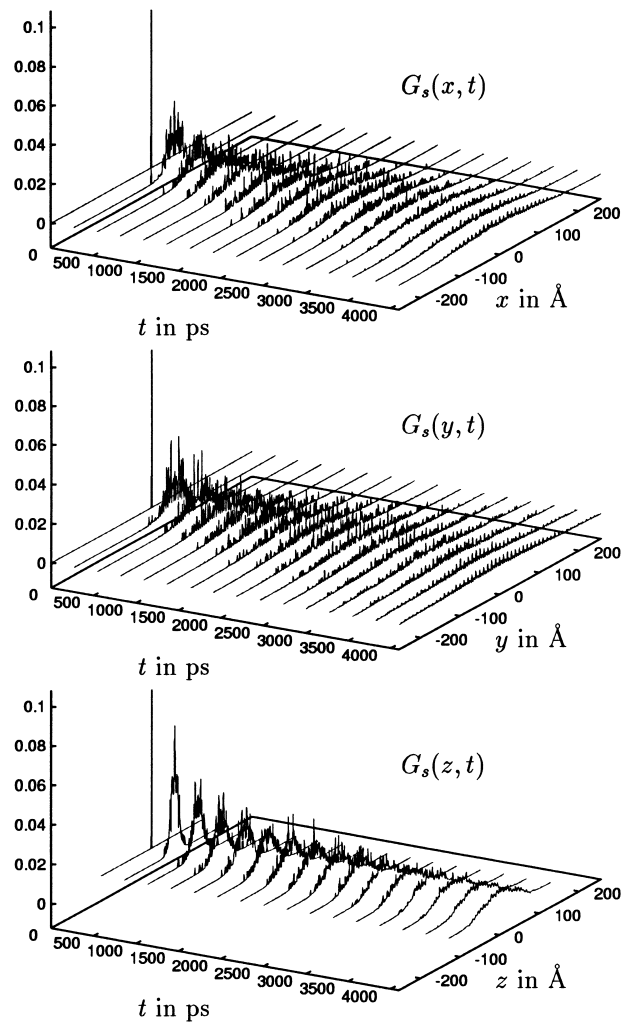


Fig. 6. Propagator (self-part  $G_s$  of the van Hove correlation function) for methane in silicalite in  $x$ -,  $y$ -, and  $z$ -direction at  $I=3$  and  $T=300$  K ( $D_x=8 \times 10^{-9} \text{ m}^2 \text{ s}^{-1}$ ,  $D_y=14 \times 10^{-9} \text{ m}^2 \text{ s}^{-1}$ ,  $D_z=1.7 \times 10^{-9} \text{ m}^2 \text{ s}^{-1}$ ).

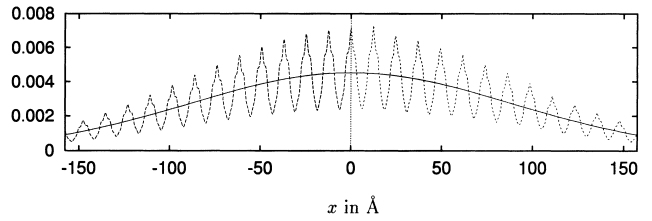


Fig. 7. Comparison of the calculated shape of  $P(x, t)$  (right-hand side) with the approximation (Eq. (6), left-hand side) for  $t=4095$  ps.  $I=3$  and  $T=300$  K.

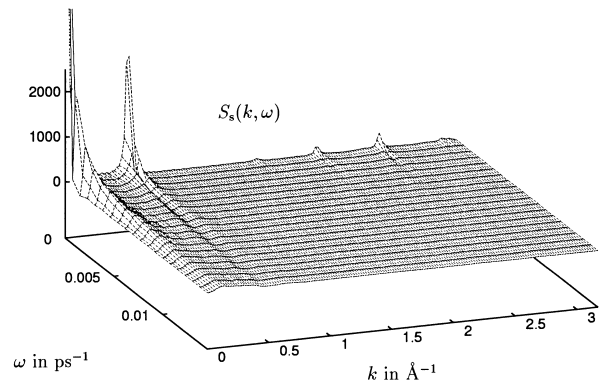


Fig. 8. Dynamic structure factor  $S_s(\mathbf{k}, \omega)$  for methane in ZK4 at  $I=3$  and  $T=300$  K.

tively. While this simple correlation rule was found to be in reasonable agreement with numerous MD simulations [11,20–23], from experimental studies only the much less definite conclusion could be drawn that the measurements were not in contrast to the correlation rule [22,24]. This is a consequence of the fact that the small size of silicalite crystallites does not allow the independent determination of the three diffusivities  $D_x$ ,  $D_y$  and  $D_z$  with the necessary accuracy.

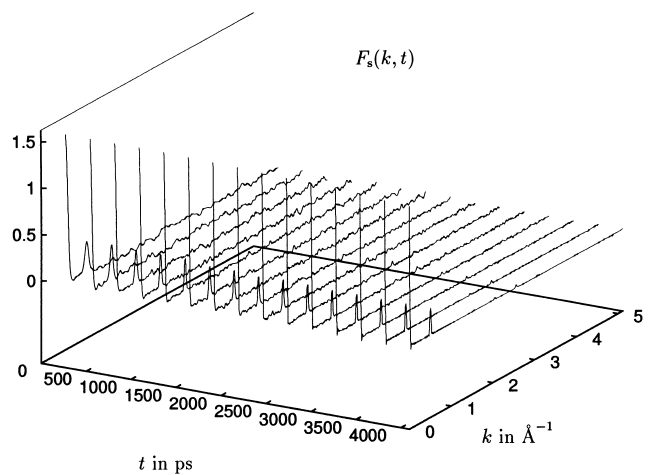


Fig. 9. Intermediate scattering function  $F_s(\mathbf{k}, t)$  for methane in ZK4 at  $I=3$  and  $T=300$  K.

In first order approximation, particle memory may be considered by an extension of Eq. (9) yielding [25]

$$\frac{c^2}{D_z} \left( 1 + \frac{2\Delta n_{sw}}{n} \right) = \frac{a^2}{D_x} \left( 1 + \frac{4\Delta n_{zz}^s}{n_z} \right) + \frac{b^2}{D_y} \left( 1 + \frac{4\Delta n_{ss}^s}{n_s} \right), \quad (10)$$

where  $n_z$  and  $n_s$  denote the number of steps along zig-zag and straight channel elements, respectively.  $n(\equiv n_z + n_s)$  is the total number of steps.  $\Delta n_{zz}^s$  and  $\Delta n_{ss}^s$  stand for the deviation of the number of step pairs carried out into the same direction along zig-zag and straight channel elements from the value expected in the case of no particle memory. Analogously,  $\Delta n_{sw}$  denotes this difference with respect to switches from one channel type to the other one. As to be expected, any enhancement of the values of  $\Delta n_{zz}^s$ ,  $\Delta n_{ss}^s$  and  $\Delta n_{sw}$  leads to an enhancement of the attributed diffusivities, viz.  $D_x$ ,  $D_y$  and  $D_z$ .

With respect to an experimental validation of correlation rules of zeolitic diffusion, chabazite (see Fig. 10) offers more promising prospects than silicalite. As a mineral, chabazite is available also with crystallites in the millimeter range. This permits the measurement of diffusion anisotropy by macroscopic orientation. Moreover, as a crystal of trigonal symmetry, chabazite may be described by a diffusion tensor of rotational symmetry around the  $z$ -axis, so that only two diffusivities,  $D_{\parallel}$  and  $D_{\perp}$ , have to be measured. Under the assumption that diffusion in chabazite is controlled by molecular passage through the windows connecting adjacent large cavities, the diffusivities parallel and perpendicular to the axis of rotational symmetry obey the relation [26]

$$\frac{D_{\parallel}}{D_{\perp}} = \frac{2h^2}{r^2} \approx 0.8, \quad (11)$$

where  $h$  and  $r$  denote the components of the separation vector (arrow in Fig. 10) between the centres of adjacent

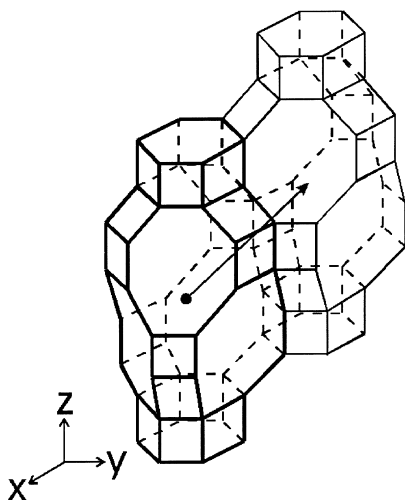


Fig. 10. Schematic representation of two adjacent large cavities of chabazite.

supercages in the direction of the symmetry axis and perpendicular to it, respectively. For diffusion studies, the chabazite crystallites have been applied in their nature-given form as provided by a deposit in the Bohemian mountains, i.e., the water contained in the crystals served as a diffusant. The PFG NMR measurements of diffusion anisotropy have been performed in two different ways, viz. (i) by macroscopically orienting the crystallites and (ii) by analysing the shape of the NMR signal attenuation in a powder sample [26]. In both sets of measurements the diffusion anisotropy was unanimously found to be  $D_{\parallel}/D_{\perp} = 0.4$ , i.e. much more pronounced than predicted by Eq. (11). Presently it cannot be decided whether this difference is due to the fact that the structure of natural chabazite crystallites may significantly deviate from the idealized homogeneous form as implied on deriving Eq. (11) e.g. by the existence of internal defects – or whether the water molecules, being much smaller than the window diameters, do not follow the basic assumption for deriving the correlation rule. It cannot be excluded that the water molecules leave the supercages preferentially through a window being on the same  $z$ -level as the window through which the cavity has been entered. In this case one clearly expects the diffusivity  $D_{\perp}$  to be enhanced in comparison with the correlation rule as given by Eq. (11).

#### 4. Single-file diffusion in zeolites

If the zeolite pore system consists of an array of parallel channels, like, e.g.  $\text{AlPO}_4\text{-5}$  or  $\theta\text{-1}$ , for sufficiently large molecules their mutual passage is excluded. Molecular transport under such conditions has been termed single-file diffusion [27–29]. After decades of mainly theoretical consideration [30–33], with the advent of zeolites with a one-dimensional pore system eventually also the experimental observation of the consequence of this type of spatial confinement has become possible. In particular it could be shown by extensive PFG NMR studies [34–37] that for sufficiently large single-file systems the molecular mean square displacements increase with the square root of the observation time,

$$\langle z(t)^2 \rangle = 2F\sqrt{t}, \quad (12)$$

rather than with the observation time itself, as it would be the case for normal diffusion. The parameter  $F$ , which has been introduced in analogy to the self-diffusivity in the Einstein equation of normal diffusion, is termed the mobility factor of single-file diffusion [28]. Eq. (12) may be considered as a special version of the more general relation [38]

$$\langle z(t)^2 \rangle = \langle |s(t)| \rangle \lambda \quad (13)$$

with  $\langle |s(t)| \rangle$  denoting the mean displacement of a single particle, if it were alone in the single-file system, and with  $\lambda$  denoting the mean free distance between adjacent molecules. A particle, alone in the system, is clearly subjected to

normal diffusion. Hence one would have

$$\langle |s(t)| \rangle = \sqrt{4Dt/\pi} \quad (14)$$

and combination with Eq. (13) reproduces Eq. (12) with  $F$  resulting as a function of the single-particle diffusivity  $D$  and the free distance  $\lambda$ :

$$F = \lambda \sqrt{\frac{D}{\pi}}. \quad (15)$$

In turn, by inverting Eq. (15), one may thus determine the diffusivity of a particle if it were alone in the single-file system. It is remarkable that these diffusivities were found to be several orders of magnitude larger than the largest so far observed diffusivities in zeolites [36]. This behaviour may be rationalized intuitively by the fact that the straight channel serves as a guide for molecular propagation ensuring that the molecular momentum (and hence the originally chosen direction of migration) is maintained much longer than it would be the case in multi-dimensional pore networks.

The validity of Eq. (12) may be corrupted very soon by the influence of the crystallite boundaries [39]. In particular it turns out that under the condition of fast particle exchange at the ends of the single-file system molecular displacement is subjected to an additional transport mechanism which follows the time dependence of ordinary diffusion

$$\langle z^2(t) \rangle = 2D_{\text{eff}}t, \quad (16)$$

where  $D_{\text{eff}}$  is related to the diffusivity  $D$  of an isolated particle in the file by the relation

$$D_{\text{eff}} = D \frac{1 - \theta}{\theta N}, \quad (17)$$

with  $N$  and  $\theta$  denoting, respectively, the site number and the site occupancy.

From a practical point of view – in particular in regard of their relevance for catalysis [40–44] – it is the rate of exchange between the intracrystalline space and the surroundings rather than the intracrystalline mobility, which deserves particular interest on considering single-file systems. Equating Eq. (16) (with Eq. (17)) and Eq. (12) (with Eqs. (13) and (14)) one finds that the time dependence of molecular displacement is very soon controlled by Eq. (15) so that the assumption might be justified that the overall exchange behaviour is controlled by an effective diffusivity given by Eq. (17). With the well-known relation

$$\tau_{\text{intra}} = L^2/12D \quad (18)$$

for the time of tracer exchange by one-dimensional diffusion between a system of length  $L$  and the environment, by insertion of Eq. (17) one would thus obtain

$$\tau_{\text{intra}} = \frac{L^3}{12Dl} \frac{\theta}{1 - \theta}, \quad (19)$$

where  $l$  denotes the site separation. In particular, the tracer exchange time would thus be expected to scale with the third power of the file length. This result is in contrast to previous

Monte-Carlo simulations [45], where for file lengths between 25 and 75 the tracer exchange time was found to scale with the power of 3.3–3.4 of the file length rather than with 3. Recently in [46] it has been shown, however, that with further increased file lengths eventually the expected scaling exponent 3 is in fact attained.

## 5. Influence of different input parameters on the evaluated diffusivity

To evaluate the desired quantities – here diffusivities – correctly, one has to choose all input parameters (model, structural data, intermolecular potentials) as appropriate as possible [47,48]. In the following we will give an estimate of the influence of the uncertainty of some of these input data on the evaluated diffusivities. Our conclusions are based on a thorough inspection of a large series of molecular dynamical (MD) simulations [11–17,22,23,47–54,62–64,67–70]:

### 5.1. Intermolecular potential

One of the most important tasks is the determination of a suitable intermolecular potential. Due to the lack of quantum chemical considerations in such complex cases [55,56], in general up to now one uses Lennard-Jones (12,6) potentials

$$U = 4\epsilon \left\{ \left( \frac{\sigma}{r} \right)^{12} - \left( \frac{\sigma}{r} \right)^6 \right\}, \quad (20)$$

with  $\epsilon$  denoting the minimum value of the potential energy and  $\sigma$  defined by  $U(\sigma)=0$  for the short-range interaction [51–54,57,58]. Quantum chemistry and the Car-Parinello method are most likely to provide more insights in the near future. A comparison with more recent experimental data [59] is very valuable too. Preliminary quantum chemical estimations [60] give values of  $\sigma$  between set A and set B in agreement with [59] justifying the phenomenological potentials.

While only slightly changing the size of the  $\sigma$ -parameter (set A into set B) the evaluated diffusivities change dramatically (including not only the absolute values but also the concentration dependence), the change of the  $\epsilon$ -parameter has essentially no influence.

It can be seen in Table 2 – where the values of  $D$  for simulations with and without interactions between methane and silicon are compared – that the influence of the silicon atoms on the diffusion is very small. Therefore most authors do in fact neglect this interaction to save computer time.

### 5.2. Vibrating lattice model

Contrary to the initial results of Suffritti and Demontis – where for the fixed and rigid lattices slightly different structure parameter are used [53,54] – the influence of

Table 2

Influence of the silicon atoms on the diffusion coefficient  $D$  ( $10^{-10} \text{ m}^2 \text{ s}^{-1}$ ) at different temperatures  $T$  (K) and for different values of the number of methane molecules per large cavity  $l$  in ZK4

$l$	$T$	With Si	Without Si
1	200	76	80
6	200	43	44
1	300	107	111
3	300	98	102
6	300	78	75
1	500	140	137
6	500	123	119

lattice vibrations on diffusion coefficients in cation-free zeolite LTA is not very large for both parameter sets under consideration [15,62]. This is shown in Fig. 11 for different  $\sigma$  (left) and different temperatures (right) [12,63,64].

### 5.3. Influence of cations on $D$

The dynamics even of small neutral molecules with saturated bindings is strongly influenced by the presence

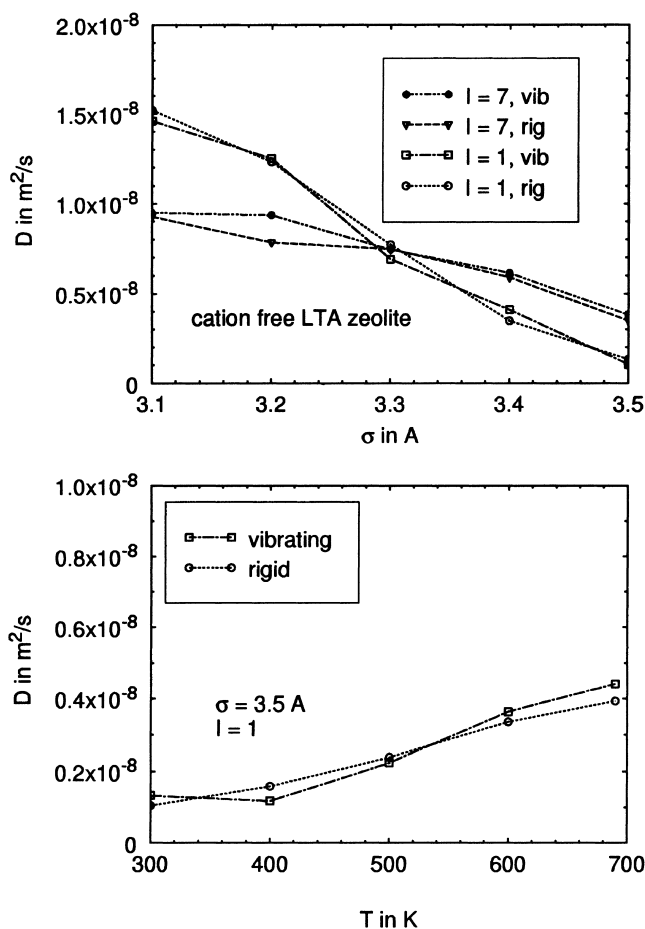


Fig. 11. Comparison of  $D$  with rigid and vibrating lattice in dependences on  $\sigma$  for two loadings (top) and in dependence on the temperature (bottom).

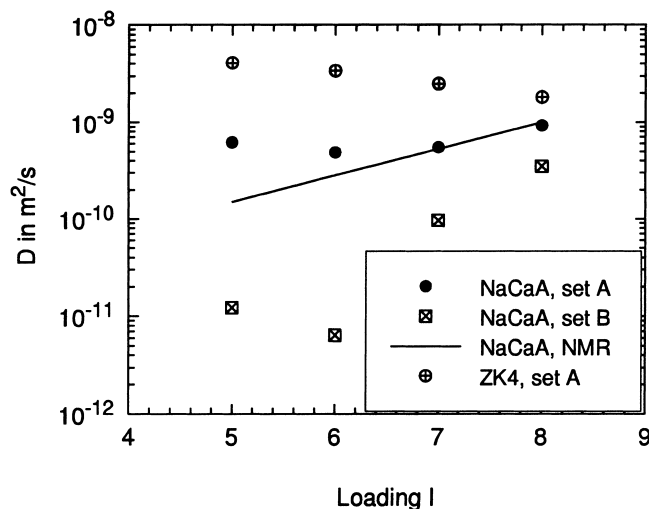


Fig. 12. Comparison of the diffusivity of methane in NaCaA and cation-free LTA as resulting from MD simulations with NMR experiments.

of exchangeable cations [67,69]. This is investigated for the NaCaA zeolite with 4  $\text{Na}^+$  and 4  $\text{Ca}^{2+}$  ions. The unexpected [65] strong effect can clearly be seen in Fig. 12 and has been confirmed experimentally, meanwhile [66]. The MD results (set A) [69] are in satisfactory agreement with experimental results from PFG-NMR measurements [61].

In comparison with the cation-free LTA, the self-diffusivity in the cation containing zeolite decreases up to two orders of magnitude (see Fig. 12). It should be noted that the computational effort is much larger in this case than in the simulations for the cation-free form since much longer trajectories (up to 5–10 ns) are necessary to evaluate such small diffusivities. Additionally, the calculation of the forces resulting from the polarization energy is very time-consuming although the full Ewald sum can be replaced by a corrected  $r$  space part of this sum [62,67,69].

## 6. Conclusion

Methods of statistical physics and molecular dynamical (MD) simulations have proved to be a helpful tool in understanding diffusion phenomena under nanoporous confinement. Among the information provided by these techniques, the propagator and its fine-structure deserve particular recognition. The confirmation of these predictions is a challenging task of further experimental studies.

## 7. Nomenclature

$\langle A \rangle$	ensemble or time average,
$\langle A(t)B(0) \rangle$	time correlation function
$a, b, c$	extensions of the unit cell
$D$	(self-) diffusion coefficient
$D_x, D_y, D_z$	diffusivities in $x$ -, $y$ - and $z$ -direction

$D_{\parallel}, D_{\perp}$	diffusivities parallel and perpendicular to the axis of rotational symmetry
$F(\mathbf{k}, t)$	intermediate scattering function
$G_s(\mathbf{r}, t)$	self-part of the van Hove auto-correlation function $G(\mathbf{r}, t)$
$n_z$ and $n_s$	number of steps along zig-zag and straight channel elements, respectively
$P(\mathbf{r}, t   \mathbf{r}_0, 0)$	(conditional) probability density that a molecule, initially at position $\mathbf{r}_0$ , will have got to position $\mathbf{r}$ at time $t$
$P(\mathbf{r}, t)$	averaged propagator
$p(\mathbf{r}_0)$	the probability density of finding a molecule at position $\mathbf{r}_0$
$\mathbf{r}$	molecular displacements during the time interval $t$
$S(\mathbf{k}, \omega)$	dynamic structure factor, ( $\mathbf{k}$ – wave vector, $\omega$ – frequency)
$U(r)$	Lennard–Jones (12,6) potential
$\epsilon$	minimum value of the potential
$\sigma$	defined by $U(\sigma)=0$

## Acknowledgements

We dedicate this paper to Prof. Dr. Harry Pfeifer on the occasion of his 70th birthday. In numerous discussions he has provided us with countless stimulations for our collaboration.

We are indebted to the Deutsche Forschungsgemeinschaft (SFB 294) for financial help.

## References

- [1] H. Pfeifer, Phys. Rep. 26 (1976) 293.
- [2] J. Kärgler, W. Heink, J. Magn. Res. 51 (1983) 1.
- [3] P.T. Callaghan, Principles of Nuclear Magnetic Resonance Microscopy, Clarendon Press, Oxford, 1991, p. 332.
- [4] L. van Hove, Phys. Rev. 95 (1954) 249.
- [5] J.P. Hansen, I.R. McDonald, Theory of Simple Liquids, Academic Press, London, 1986.
- [6] L. van Hove, Physica 24 (1958) 404.
- [7] J. Kärgler, D.M. Ruthven, Diffusion in Zeolites and Other Microporous Solids, Wiley, New York, 1992.
- [8] M. Bée, Quasielastic Neutron Scattering, Adam Hilger, Bristol, 1988.
- [9] H. Jobic, in: B. Imelik, J.C. Vedrine (Eds.), Catalyst Characterization: Physical Techniques for Solid Materials, Plenum Press, New York, 1994, p. 347.
- [10] T. Springer, in: J. Kärgler, P. Heitjans, R. Haberlandt (Eds.), Diffusion in Condensed Matter, Vieweg, Wiesbaden, 1998, p. 59.
- [11] M. Gaub, Ph.D. Thesis, Leipzig University, 1998.
- [12] R. Haberlandt, Thin Sol. Films 330 (1998) 46.
- [13] R. Haberlandt, in: J. Kärgler, P. Heitjans, R. Haberlandt (Eds.), Diffusion in Condensed Matter, Vieweg, Wiesbaden, 1998, p. 363.
- [14] M. Gaub, S. Fritzsche, R. Haberlandt, D.N. Theodorou, Van Hove function for the diffusion in zeolites, submitted to J. Phys. Chem. B.
- [15] S. Fritzsche, M. Gaub, R. Haberlandt, G. Hofmann, J. Mol. Model. 2 (1996) 286.
- [16] A. Schüring, Diploma Thesis, Leipzig, 1997.
- [17] A. Schüring, S. Fritzsche, R. Haberlandt, D. Michel, Ethane in LTA-type zeolites – An MD Study, in preparation.
- [18] J. Kärgler, J. Phys. Chem. 95 (1991) 5558.
- [19] J. Kärgler, H. Pfeifer, Zeolites 12 (1992) 872.
- [20] R.L. June, A.T. Bell, D.N. Theodorou, J. Phys. Chem. 94 (1990) 8232.
- [21] P. Demontis, E.S. Fris, G.B. Suffritti, S. Quartieri, J. Phys. Chem. 94 (1990) 4329.
- [22] S. Jost, S. Fritzsche, R. Haberlandt, Chem. Phys. Lett. 279 (1998) 385.
- [23] S. Jost, N.K. Bär, S. Fritzsche, R. Haberlandt, J. Kärgler, J. Phys. Chem. B 102 (1998) 6375.
- [24] U. Hong, J. Kärgler, H. Pfeifer, U. Müller, K.K. Unger, Z. Phys. Chem. 173 (1991) 225.
- [25] J. Kärgler, P. Demontis, G.B. Suffritti, A. Tilocca, J. Chem. Phys. 101 (1999) 1163.
- [26] N.-K. Bär, J. Kärgler, H. Pfeifer, H. Schäfer, W. Schmitz, Micro. Mesopor. Mat. 22 (1998) 289.
- [27] L. Riekert, Adv. Catal. 21 (1970) 289.
- [28] J. Kärgler, M. Petzold, H. Pfeifer, S. Ernst, J. Weitkamp, J. Catal. 136 (1992) 283.
- [29] J. Kärgler, G. Fleischer, U. Roland, in: J. Kärgler, P. Heitjans, R. Haberlandt (Eds.), Diffusion in Condensed Matter, Vieweg, Wiesbaden, 1998, p. 144.
- [30] P.M. Richards, Phys. Rev. B 16 (1977) 1393.
- [31] H. van Beijeren, K.W. Kehr, R. Kutner, Phys. Rev. B 28 (1983) 5711.
- [32] J. Kärgler, Phys. Rev. A 45 (1992) 4173.
- [33] J. Kärgler, Phys. Rev. E 47 (1993) 1427.
- [34] V. Gupta, S.S. Nivarthi, A.V. McCormick, H.T. Davis, Chem. Phys. Lett. 247 (1995) 596.
- [35] V. Kukla, J. Kornatowski, D. Demuth, I. Girmus, H. Pfeifer, L.V.C. Rees, S. Schunk, K.K. Unger, J. Kärgler, Science 272 (1996) 702.
- [36] K. Hahn, J. Kärgler, V. Kukla, Phys. Rev. Lett. 76 (1996) 2762.
- [37] D. Keffer, A.V. McCormick, H.T. Davis, Mol. Phys. 87 (1996) 367.
- [38] K. Hahn, J. Kärgler, J. Phys. A 28 (1995) 3061.
- [39] K. Hahn, J. Kärgler, J. Phys. Chem. B 102 (1998) 5766.
- [40] Z. Karpinski, S.N. Ghandi, W.M.H. Sachtler, J. Catal. 141 (1993) 337.
- [41] G.D. Lei, B.T. Carvill, W.M.H. Sachtler, Appl. Catal. 142 (1996) 347.
- [42] G.D. Lei, W.M.H. Sachtler, J. Catal. 140 (1993) 601.
- [43] C. Rödenbeck, J. Kärgler, K. Hahn, J. Catal. 176 (1998) 513.
- [44] C. Rödenbeck, J. Kärgler, K. Hahn, W.M.H. Sachtler, J. Catal., in press.
- [45] C. Rödenbeck, J. Kärgler, K. Hahn, J. Catal. 157 (1995) 656.
- [46] C. Rödenbeck, J. Kärgler, K. Hahn, J. Chem. Phys. 110 (1999) 3970.
- [47] M.P. Allen, D.J. Tildesley, Computer Simulation of Liquids, Clarendon Press, Oxford, 1989.
- [48] R. Haberlandt, S. Fritzsche, G. Peinel, K. Heinzinger, Molekulardynamik-Grundlagen und Anwendungen, with a chapter about Monte-Carlo-Simulation by H.L. Vörtler, Vieweg, Wiesbaden, 1995.
- [49] D.N. Theodorou, R.Q. Snurr, A.T. Bell, in: G. Alberti, T. Bein (Eds.), Comprehensive Supramolecular Chemistry, vol. 7, Pergamon Press, Oxford, 1996, p. 507.
- [50] P. Demontis, G.B. Suffritti, Chem. Rev. 97 (1997) 2845.
- [51] S. Fritzsche, R. Haberlandt, J. Kärgler, H. Pfeifer, M. Wolfsberg, Chem. Phys. Lett. 171 (1990) 109.
- [52] S. Fritzsche, R. Haberlandt, J. Kärgler, H. Pfeifer, K. Heinzinger, Chem. Phys. Lett. 198 (1992) 283.
- [53] P. Demontis, G.B. Suffritti, Chem. Phys. Lett. 223 (1994) 355.
- [54] P. Demontis, G.B. Suffritti, in: J. Weitkamp, H.G. Karge, H. Pfeifer, W. Hoelderich (Eds.), Proceedings of the 10th International Zeolite Conference, Elsevier, Amsterdam, 1994, NL, p. 2107.
- [55] J. Sauer, in: Molecular Electronic Structure Theory, vol 2, JAI Press, 1994, p. 111.

- [56] J. Sauer, *Stud. Surf. Sci. Catal.* 84 (1994) 2039.
- [57] A.G. Bezus, A.V. Kiselev, A.A. Lopatkin, P.Q. Du, *J. Chem. Soc., Faraday Trans. II* 74 (1978) 367.
- [58] J.O. Hirschfelder, C.F. Curtiss, R.B. Bird, *Molecular Theory of Gases and Liquids*, Wiley, New York, 1954.
- [59] B. Smit, *J. Chem. Phys.* 99 (1995) 5597.
- [60] A. Schüring, D. Heidrich, R. Haberlandt, in preparation.
- [61] W. Heink, J. Kärger, H. Pfeifer, P. Salverda, K.P. Datema, A. Nowak, *J. Chem. Soc., Faraday Trans.* 88 (1992) 515.
- [62] S. Fritzsche, *Habilitationsschrift*, Leipzig University, 1998.
- [63] S. Fritzsche, M. Wolfsberg, R. Haberlandt, P. Demontis, G.B. Suffritti, A. Tilocca, *Chem. Phys. Lett.* 296 (1998) 253.
- [64] S. Fritzsche, M. Wolfsberg, R. Haberlandt, *The Thermalization Effect of Lattice Vibrations and Mutual Interaction in a Cation-free LTA Zeolite*, to be published.
- [65] General Discussion, *J. Chem. Soc., Faraday Trans.* 87 (1991) 1797.
- [66] W. Heink, J. Kärger, S. Ernst, J. Weitkamp, *Zeolites* 14 (1994) 320.
- [67] S. Fritzsche, R. Haberlandt, J. Kärger, H. Pfeifer, M. Waldherr-Teschner, *Stud. Surf. Sci. Catal.* 84 (1994) 2139.
- [68] S. Fritzsche, *Phase Transitions* 52 (1994) 169.
- [69] S. Fritzsche, R. Haberlandt, J. Kärger, H. Pfeifer, K. Heinzinger, M. Wolfsberg, *Chem. Phys. Lett.* 242 (1995) 361.
- [70] S. Fritzsche, R. Haberlandt, J. Kärger, H. Pfeifer, K. Heinzinger, *Chem. Phys.* 174 (1993) 229.